Multispectral MR Imaging and Sensing Using Shaped Nanoparticles

Gary Zabow

1 Introduction

The discovery of fluorescent proteins and their application in bioimaging have significantly advanced molecular and cellular biology [1–3]. Color-labeling with such fluorophores enables distinction between different cell types and different biomolecules, allows multiplexing and high-throughput bioassays, supports colorimetric sensing for real-time visualization of biomolecular processes and functions, and is critical to a host of new superresolution microscopy techniques [4, 5]. In addition to such molecular labels and probes, the bioimaging revolution that they started is now driven also by multicolor nanoparticle-based analogs. Prominent among these are semiconductor nanocrystal quantum dots [6–9], metallic plasmonic nanostructures [10, 11], and more recently nanodiamonds [12] and related carbon-based, low-toxicity fluorescent nanoparticles [13].

Despite unquestioned utility, however, optical probes still suffer from limited in vivo functionality, where optical access is more challenging or entirely precluded. The growing realization that optically accessible in vitro, or largely two-dimensional, testing does not accurately mimic more realistic, three-dimensional, in vivo physiological conditions, neither chemically nor mechanically [14], has spurred much research into extending optical penetration depths through biological tissues [15]. Among others, this includes confocal [16] and two- or multiphoton imaging schemes [17, 18], photoacoustic imaging [19], and adaptic-optic wavefront-shapings that can dynamically refocus light through turbid, scattering media [20, 21]. Concurrently, optical

G. Zabow (✉)
Applied Physics Division, National Institute of Standards and Technology (NIST),
325 Broadway, Boulder, CO 80305, USA
e-mail: zabow@boulder.nist.gov

J.W.M. Bulte, M.M.J. Modo (eds.), *Design and Applications of Nanoparticles in Biomedical Imaging*, DOI 10.1007/978-3-319-42169-8_5

nanoparticle probes are being reengineered with resonances shifted towards the more favorable near-infrared region of the spectrum where biological phototoxicity is reduced and intervening biological media offer less photon attenuation and less interfering background autofluorescence [22, 23]. Even so, optical signal intensities and spatial resolutions still fall rapidly with increasing depth below the surface.

For in vivo probing, magnetic resonance imaging (MRI) would seem an ideal alternative were it not for its largely monochromatic nature that forfeits many of the multicolor advantages that make multispectral optical probes so valuable in the first place. MRI is a powerful imaging technology that offers safe, deep in vivo imaging with excellent soft-tissue contrast and high spatial resolution compared to other radiological imaging modalities [24]. Not requiring any ionizing radiation, it has become one of the most widely accepted medical imaging and diagnostics tools. Operating in the radio-frequency range, MRI can noninvasively penetrate tissue without signal loss or distortion and is inherently immune to background autofluorescence, photobleaching, and phototoxicity issues that plague optical imaging. Moreover, MRI has the capability to discern not only anatomical form but also physiological function through many unique contrast mechanisms that provide sensitivity to such key variables as water diffusion [25–27], paramagnetic metal ion content (particularly iron [28]), and blood flow [29], perfusion [30], and oxygenation levels [31]. Even in vivo cellular and molecular level information is becoming accessible through an ever-growing array of targeted, and even genetically expressed, MRI contrast mechanisms [32]. These enable in vivo probing of many biomarkers and include early-stage disease detection through cell-type or epitope recognition [33–36] and imaging of gene expression and enzyme activity [37–41].

However, MRI has traditionally lacked the multiplexing advantages of multicolor optical imaging modalities. Images typically comprise amplitude (and/or phase) maps of the local water signal, determined by the local density of water and its movement and relaxation properties, which enable a rich array of different contrast mechanisms. Nevertheless, just as optical colors represent different wavelengths or optical frequencies, a color MRI mapping requires also some analogous form of frequency-based distinction. NMR spectroscopy already does just that, identifying different chemical molecules through their different NMR spectra and to some extent this chemical-shift information carries over to MRI through chemical-shift imaging and magnetic resonance spectroscopy (MRS). But in vivo MRS sensitivities are low, enabling high-resolution imaging of only those biomolecules that naturally occur in sufficiently high concentrations [42, 43].

This historical lack of multiplexed image contrast has not only impeded potential in vivo multiplexing applications, but also limited quantitative accuracy of MRI analyses (discussed below). Recognizing such weaknesses, several new multispectral approaches to MRI contrast have been advanced in recent years including agents based on chemical exchange and on ^{19}F, offering some of the first MRI multiplexing alternatives that sidestep optical access limitations of optical reporters. One of the most recent approaches—the focus of this chapter—uses magnetic nanoparticles whose special shapes enable multispectral MRI labeling and sensing. To place these new multispectral shaped contrast agents into better context, however, other multispectral, as well as more traditional, approaches to MRI contrast are first discussed.

Many excellent reviews already exist on the topic of MRI contrast agents [44, 45]; thus here only a brief overview is given.

2 MRI Contrast Agents

In addition to the many endogenous contrast schemes accessible to MRI, the clinical success of MRI owes much to the invention of exogenous contrast agents, which may be either molecular or nanoparticle based. Roughly a third of all clinical MRI exams currently employ an administered exogenous contrast agent, amounting to some 10 to 20 million contrast agent-enhanced exams annually. Such agents are regularly employed to highlight blood flow and detect abnormal, damaged tissue, perhaps most notably including detection of blood-brain barrier disruption and the presence of brain tumors [46].

2.1 T_1 and T_2 Agents

By far the most common clinical MRI contrast agents are molecular paramagnetic agents based on chelates of the Gd^{3+} ion [47, 48], although agents based on Mn^{2+}, which can directly enter cells, are also used [49–51]. With seven unpaired electrons, the relatively large, fluctuating magnetic fields around Gd^{3+} ions can significantly affect both the longitudinal (T_1) and transverse (T_2) relaxation rates of hydrogen protons in closely neighboring water molecules. Because their relative effect on T_1 is larger, however, Gd-chelates are generally referred to as T_1 contrast agents and used with T_1 image-weighting schemes. By rapidly repeating image acquisitions, these T_1-weighted images exploit the locally reduced longitudinal relaxation time, T_1, of the nearby water protons to increase image brightness or signal (positive contrast) near the contrast agent as compared to the weaker signal accrued from more slowly relaxing water protons further away.

Many nanoparticle-based contrast agents also exist. These include nanoparticles of manganese oxide [52, 53], of gadolinium oxide [54, 55], and, most prominently, of superparamagnetic iron oxide (SPIO) that benefit from many already-developed synthesis methods [56, 57]. SPIO nanoparticles contain magnetite (Fe_3O_4) or maghemite (γ-Fe_2O_3), which offer much greater magnetic moments than chelated paramagnetic ions. Therefore, they can affect water relaxivity out to relatively large distances, much greater than the contrast agent particle sizes, which themselves span a large range from a few nanometers up to a few micrometers. They include nanometer-sized monocrystalline iron oxide nanoparticles (MIONs) [58] and ultrasmall SPIO (USPIO) [59] agents (often dextran coated for biocompatibility and solubility), as well as assorted agglomerations thereof that include magnetodendrimers [60] a few tens of nanometers in size, larger composite SPIO agents [61, 62] up to a few hundred nanometers in diameter, and even micrometer-scale particles of iron oxide (MPIOs) that may be as large as several micrometers across [63] and that

can be individually detected [64]. While these particulate-based agents also affect both T_1 and T_2, they are referred to as T_2 contrast agents since their effect on T_2 is far greater, especially as particle sizes increase. For T_2 agents, the inhomogeneous magnetic fields surrounding the nanoparticles cause a transverse dephasing of surrounding hydrogen proton spins that increases over time. Independent of any longitudinal relaxation, this loss of transverse spin coherence locally reduces signal intensity or image brightness, yielding "negative contrast" near the nanoparticles (although schemes do exist to provide also positive contrast [65, 66]). Distinct from T_1-weighted imaging, T_2-weighted imaging therefore seeks to reduce image repetition rates, using longer repeat and echo times to enhance the amount of dephasing, accentuating the local image darkening in the contrast agent vicinity. Although negative T_2 contrast agents are clinically less common than positive T_1 agents, they have been used for in vivo liver imaging [67, 68]. They are also widely used in preclinical studies, in particular in MRI cell tracking [69–73], for which their magnetic field disturbances are large enough to enable single-cell detection in vitro [74–76] and even in vivo [77]. Additionally, superparamagnetic nanoparticles are employed in magnetic resonance-based bioassays through relaxation switch sensors that detect molecular binding events [78], and thereby analyte concentrations [79], through particle aggregation-dependent changes in T_2 relaxation rates [80].

Regardless of whether contrast agents are molecular or nanoparticle based, however, the net result of T_1 and of T_2 relaxation enhancers is a change in image brightness or amplitude. Such signal amplitude changes are analogous to brightness or intensity changes of optical imaging probes; what these T_1 and T_2 relaxation schemes lack is some equivalent to the different color, or, effectively, different optical frequency information, available to optical probes. Being solely amplitude based complicates distinction between different types of MRI contrast agents that may be simultaneously present; to some extent distinguishing between a T_1 and a T_2 agent is possible [81], but this falls short of the multiplexing capabilities of colored probes accessible to optical imaging modalities. This lack of distinction between different agent types also hinders quantitative signal analyses. Without a priori knowledge of the exact amount of contrast agent present, changes in signal intensity may result from a change in contrast agent concentration rather than in the quantity or functioning of some targeted biological variable under study. Distinguishable agents, on the other hand, may allow for ratiometric measures that eliminate concentration dependences, provided that the distinguishable agents are themselves present in some known concentration ratio to each other and are similar enough that they are tracked the same way through the body.

2.2 Heteronuclear Agents

Besides relatively low-sensitivity MRS, one spectroscopic approach to distinguishing between different agents is to base those agents on MRI-detectable nuclei other than the hydrogen protons used in conventional ^{1}H MRI. Fluorinated compounds, for example, which are inert, nontoxic, and based on highly NMR-sensitive ^{19}F

nuclei (comparable to ^{1}H nuclei sensitivity), have long been used as contrast agents or, better formulated, tracers [82, 83], easily predating all Gd^{3+} and magnetic nanoparticle T_1 and T_2 agents by several years [84]. Substrates labeled with hyperpolarized ^{13}C [85, 86] also find much use, particularly in metabolic imaging. Other common NMR-active nuclei include ^{15}N, ^{31}P, and noble gases like ^{129}Xe. And Si nanoparticles containing hyperpolarized ^{29}Si have also been recently introduced as possible MRI tracers [87]. Different nuclei have different gyromagnetic ratios. Therefore, unlike T_1 and T_2 agents, which alter water relaxivities, heteronuclear agents are detected at completely different resonance frequencies, well separated from those of water. They can therefore be distinguished from each other and from conventional contrast agents and, for cases like ^{19}F where there is negligible naturally occurring free fluorine in the body, offer the advantage of background-free detection and even a form of ^{19}F-based multispectral MRI [88].

Still, compared to available water (with hydrogen nuclei concentration up to 110 M), exogenous heteronuclear agents, even hyperpolarized and/or background free, would need to be administered in very high concentrations to match the signal-to-noise ratios achievable with ^{1}H MRI. This is not only because other nuclei may be less NMR sensitive than hydrogen, but also because for heteronuclear agents it is the agent itself that is being detected, whereas for ^{1}H contrast agents it is not the contrast agent, but instead the nearby water that is being detected. That is, T_1 and T_2 contrast agents benefit from interacting with large amounts of water to significantly boost their effective signals, albeit at the expense of no frequency discrimination between these signals.

2.3 Chemical Exchange Agents

An alternative approach that has enjoyed rapid growth over the past decade is the field of chemical exchange saturation transfer (CEST) agents [89] and their paramagnetic equivalents (PARACEST) [90]. Like T_2 contrast agents, CEST agents interact with the surrounding water to decrease the ^{1}H signal, but CEST agents are able to provide signals at different offset frequencies from the background water. They do this by exploiting proton exchange, a natural chemical exchange process whereby weakly bound protons on certain molecules continually exchange with free (unbound) protons in the surrounding bulk water. While attached, the protons experience a chemical shift due to the molecule that they are (temporarily) a part of. Irradiation at that particular chemically shifted offset frequency allows the magnetization of the bound protons to be selectively "saturated out" while leaving the unbound water untouched. When the bound protons subsequently exchange with the surrounding free water protons, they reduce the total magnetization then detected in the unbound water signal. A full magnetization saturation spectrum, referred to as a z-spectrum [91], can then be acquired by repeating the presaturing irradiation pulses over a series of different offset frequencies. Depending on how rapidly chemical exchange recurs, the off-resonance irradiation process can be repeated multiple times within the free water's T_1 relaxation time, multiplying the number of

protons that can be magnetically saturated out and boosting the resulting difference in on-resonance signal magnitude. Thus the CEST effect provides an indirect, but clever way to amplify the frequency-shifted signatures of certain molecules that might otherwise yield only weak signal or be undetectable with magnetic resonance spectroscopy imaging. CEST imaging does still require high concentrations of exchanging protons but, fortuitously, some biomolecules with the necessary labile protons do naturally occur at high concentrations and are therefore amenable to such CEST imaging protocols [92]. This gives CEST the advantage of being applicable to both endogenous and exogenous contrast enhancement schemes.

One route to reducing required CEST concentrations is to use molecules with higher proton exchange rates, thus amplifying the signal per molecule. Proton exchange does broaden the shifted linewidths, however, limiting the useful frequency of exchange to of order the chemical frequency shift itself, the so-called "slow exchange" limit [93]. CEST molecules with as large a chemical shift as possible are therefore sought, but many candidate endogenous CEST molecules are diamagnetic offering relatively small shifts. These shifts are proportional to the magnetizing field of the MRI scanner and can thus to some extent be increased by working at higher fields, but this puts many potential applications out of clinical reach. Another workaround is to use exogenous CEST agents that include paramagnetic ions. These PARACEST agents generate larger frequency shifts that allow for more rapid proton exchange and aid in discriminating signals from the background water and from each other.

Whether CEST or PARACEST, their ability to generate signals at different frequency offsets allows for selectively addressable contrast and simultaneous use of more than one agent type, enabling a form of multispectral image contrast [94–96]. Many versions of PARACEST agents are currently being explored, including polymer and supramolecular versions [97, 98], liposome-based LIPOCEST agents [99], and even hyperpolarized (HYPERCEST) systems [100]. Promising as these CEST agents are, all are ultimately limited by their chemical shifts and by the number of exchangeable protons on the molecules used. As recently shown [101], however, NMR frequency shifts need not be restricted to only those from molecular chemical shifts or differing nuclear gyromagnetic ratios; NMR frequency shifts can also be engineered through a new class of contrast agents based on specially shaped magnetic nano- and microparticles.

3 Shaped Nanoparticles

An overwhelming majority of nanoparticles are spherical. This is not surprising. Without deliberate intention otherwise, energy minimization automatically renders many chemically synthesized particles roughly spherical in form. For many applications, it is also more size than shape that matters anyway. Often size is the fundamental determinant of novel nanoparticle functionality due to quantum effects that increasingly dominate over classical ones as particle sizes shrink. In other cases, size dominates simply because the decreasing footprints of nanoparticles make them less obtrusive, a key requirement in, for example, many biomedical applications.

But as the fields of nanotechnology mature—particularly the subfields of nanoparticle synthesis and related colloid and self-assembly research—appreciation of the unique functionalities enabled by nonspherical particles and new ways to synthesize them are growing [102, 103]. Nanoparticle shapes now comprise a veritable zoo of nanocreatures including such species as nanorods, nanotubes, nanorings, nanoshells, nanocubes, nanoellipsoids, nanopyramids, nanodisks, nanobelts, nanocylinders, nanoribbons, nanodumbbells, nanodiscoballs, nanopeanuts, nanostars, nanoscrews, nanocoils, nanosprings, nanotetrapods, nano-octapods, nanohexagons, nanobarrels, nanocages, nanomushrooms, nanoflowers, nanocrescents, nanoworms, and more besides including even such curiously sounding recent proposals as drug-delivering nanovolcanoes [104]. To be sure, many have yet to find any actual use. But among those that have, the applications enabled specifically by nonspherical particles are many and varied. They span a range of fields too broad to cover here, from enhanced platinum nanoparticle catalysis [105] to self-assembled materials with unique anisotropic optical and mechanical properties [106–108]. Even limited to biomedical fields, applications are numerous. Nanoparticle shape—not just size or surface charge—has been found to influence cell uptake rates [109–111], prolong in vivo circulation times and improve tumor targeting efficiency [112], and enhance preferential targeting of particular cell/tissue types [113]. Optical resonances, local electric field enhancements, and heating properties of metallic plasmonic nanoparticles [114–116], which find use in biomedical imaging, sensing, and potential photothermal therapies, are directly determined by both nanoparticle size and shape. And shaped magnetic particles are also attracting attention. Whereas spherical magnetic particles can only translate in a magnetic field, the shape anisotropy of nonspherical particles allows them to be also rotated. This is advantageous because translational magnetic forces, which depend on gradients in the magnetic field, often require close proximity to the source magnet and may be weaker than magnetic torques, which depend on the magnetic field strength itself. Thus asymmetric and corkscrew-shaped magnetic microparticles underpin much of the new field of so-called magnetic swimmers [117], which transduce externally applied magnetic field rotation into mechanical translation with a goal of magnetically guided drug delivery. New ways to attack cancer cells have also been proposed using targeted thin disk-shaped particles whose magnetic shape anisotropy allows them to be rapidly oscillated back and forth to destroy the cells to which they are attached [118]. As a further illustration, increased anisotropy of cube-shaped magnetic nanoparticles has been argued to enhance heat absorption over equivalent spherical particles for alternative magnetic hyperthermia approaches to treatment [119].

3.1 Shaping NMR Relaxivity

In MRI, deliberately shaped nanoparticles are less conspicuous, but not entirely absent either. To be sure, for T_1 and T_2 contrast agents, size is the more important qualifier than shape: smaller, molecular scale agents make better T_1 relaxers, while larger nano- and microparticles with higher magnetic moments excel at T_2 contrast generation. Changing size not only changes relaxation efficiency, but can even

switch between predominantly T_1 and T_2 relaxation. For example, T_2 MnO particulate contrast agents transform into T_1 agents by releasing free manganese ions when dissolved in acidic cellular endosomes/lysosomes [120]. Conversely, T_1 Gd chelates become better T_2 relaxers when locally concentrated together.

But shape itself can also play a role. One recent example claims increased T_2 contrast through the use of octapod-shaped iron oxide nanoparticles [121], where the more pointed structure gives a more disperse distribution of material with a larger fraction of the magnetic material positioned further from the particle center than would be the case for a solid sphere. It is argued that the more open structures and effectively increased particle diameters allow the nanoparticles to interact with more water, increasing the transverse relaxivity. A comparable case for T_1 contrast agents may be recent Gd(III)-DNA-coated gold nanostars [122] showing increased T_1 contrast (compared to Gd(III)-DNA-coated spheres, for example), believed due at least in part to improved water access resulting from their nonspherical star shapes. Although contrast mechanisms differ, in both cases moving away from a spherical shape to one that is more open with higher curvature surfaces appears to increase water access and relaxivity. Gadolinium-containing ultrashort carbon nanotubes [123] represent another relatively new, and patently nonspherical, set of MRI contrast structures under development. They show significantly higher MR relaxivities than traditional agents, thought due to nanoscale clustering of Gd^{3+} ions confined within the nanotubes and, again, higher water access [124]. This is not to say that relaxivities are necessarily optimized through particles that are specifically octapod-, star-, or tube shaped, but it does show that nanoscale shape can be important.

4 Geometrically Based Multispectral MRI Contrast

The above examples increase image contrast; to add distinguishing spectral content a different approach dependent on more specifically designed, shaped magnetic microstructures was recently introduced [101]. Here the spectral information was a direct consequence of the precise magnetic geometries used, enabling controlled NMR frequency shifting, multiple uniquely identifiable contrast agents, and the prospect of larger scale multiplexing with MRI. Unlike the above nanostructure agents, these multispectral contrast agent structures do not necessarily need to be nanoscale; their operation, while highly dependent on particle shape, is to a large extent size independent.

4.1 Using Shape to Control Frequency

Because all magnetic particles add T_2 contrast, regardless of shape, it helps revisiting how that contrast is generated to better understand how particle geometries can also encode distinct spectral signatures. In a pure water sample free of any magnetic

particles, the hydrogen proton spins all precess at the same Larmor frequency, which is proportional to the magnitude of the magnetic field of the MRI scanner. Once a magnetic particle is added to the water its own surrounding magnetic field adds to the MRI field, altering the precession frequencies of protons nearby. Because the particle field is different in different positions around the particle, precession frequencies differ between neighboring water molecules. Thus proton spins accrue different transverse phases with respect to one another, leading to destructive signal interference that locally darkens the image around the particle location. Or, spectrally, the NMR line is broadened since signal from around the particle introduces a continuous spread in precession frequencies.

Such contrast is largely independent of particle shape. What makes magnetic microparticles such powerful T_2 relaxers is the large distances out from the particle over which the particle magnetic field can cause appreciable transverse dephasing. Fields from a single micrometer-sized particle, for example, may be sufficiently strong to significantly dephase hydrogen protons out to of order 100 μm away from that particle [125], encompassing a volume of water many orders of magnitude larger than that of the particle itself. Therefore, unlike T_1 contrast that only relaxes water close to the agent—in the first or second coordination sphere of the paramagnetic ion used—for larger agents much T_2 contrast accrues from water relatively far from the particle. At such distances, any higher spatial frequency components, or equivalently higher multipole moments, in the surrounding particle field distribution have decayed away. Transverse dephasing due to microparticles is therefore predominantly due to spatially decaying dipole fields that, while proportional to net particle magnetic moment and/or size, retain no other information about particle shape.

Avoiding such dephasing, which blurs any potential distinguishing spectral content, requires instead a spatially extended region about the magnetic particle over which the magnetic field does not change. Within such a uniform field region, the precession frequencies of water protons would all be the same, locally keeping all proton spins in phase. This would locally avoid NMR line broadening, but would frequency-shift the water line proportionally to the shifted field magnitude within that region. Such a field setup might initially seem unlikely but, even though all magnetized particles project dipolar far fields, this does not preclude generating the necessary uniform field in the near-field regions of specially designed magnetic microstructures. Further, since signals from water within such a near-field region are spectrally distinct from water further away, selective signal amplification becomes possible. Thus large signals can still be acquired from the engineered uniform near-field volumes even though those water volumes may be much smaller than their dipole-field-dominated far-field counterparts.

4.2 Frequency-Shifting Micromagnetic Structures

As a concrete example, Fig. 1 shows one possible microstructure that can discretely shift the NMR frequency of nearby water. It consists of two magnetizable disks, spaced a distance apart roughly equal to the disk radii. When magnetically saturated

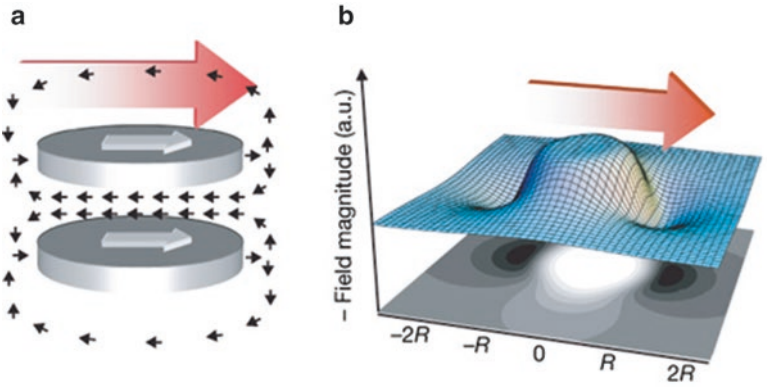

Fig. 1 Double-disk magnetic structure and field diagrams. (**a**) Schematic of the field (small *black arrows*) from two parallel disks magnetized to saturation by the background field of an MRI scanner (large *red arrow*). Nonmagnetic spacer elements are omitted for clarity. (**b**) Calculated (negative) field magnitude in the mid-plane through a typical magnetized disk set, contrasting its homogeneous nature between the disks with its rapid external decay (reproduced in part from [101], with permission, Nature Publishing Group)

in a typical MRI scanner, this particle geometry yields an extended spatial region between the disks where the field is roughly uniform and of a different magnitude to the fields far away from the particle. Note that this does not eliminate the dipolar field decay external to the structure. The dipole field still exists, dephasing surrounding water and broadening the NMR water line just like any other T_2 agent. But within the inner uniform field region, there is a volume of water where all proton spins precess at the same offset frequency, different to the resonance frequency of the bulk water signal. The structure therefore adds a distinct frequency-shifted peak to the acquired NMR spectra. The frequency shift, $\Delta\omega$, is proportional to the difference in magnitudes of the field between the disks and the field far away where water is unperturbed by their presence. The uniform field generated by the disks can be approximated analytically from the field at the center point of the structure. For magnetically saturated disks of thickness h, radius r, center-to-center separation $2S$, made from material with a saturation magnetic polarization density J_S, and immersed in a medium of gyromagnetic ratio γ, the resulting NMR frequency shift is [101]

$$\Delta\omega \approx -\gamma J_S\left(\frac{h r^2}{2(r^2+s^2)^{3/2}}\right)$$

where thin disks with $h << 2S \approx R$ are assumed for simplicity. Different frequency offsets can therefore be engineered by changing the magnitude of the field between the disks. This can be done by changing the spacing between the disks, the disk radii, the disk thicknesses, or the magnetic material from which the disks are made. All of these variables can be controlled when microfabricating such structures, allowing tailored frequency shifts over large frequency ranges. Thus families of

structures can be created, each capable of offsetting the water NMR frequency by a different amount. These frequencies lie in the NMR radio-frequency (RF) range, but if each different frequency offset is associated with a different color (as in the optical spectrum) multispectral, or "RF color," contrast becomes possible. Although operational principles are different, in many ways such shaped magnetic particles become RF analogues to optical quantum dots, or plasmonic nanoparticles. All have resonances that can be engineered by controlling either the size of the quantum dots, the size and shape of the plasmonic nanoparticles, or the geometrical aspect ratios of the magnetic nano- or microparticle structures.

Double-disks are not the only structures that can frequency-shift the NMR signal. As mentioned, the main requirement is generating a uniform offset field region and this can be done in more than one way. For example, short, hollow cylindrical tubes with a length approximately equal to their diameter can also generate the necessary water-accessible, spatially extended regions of uniform field offset within their interior [126]. Figure 2 shows an example of the fields of such a structure which give frequency shifts of [126]

$$\Delta\omega \approx -\gamma J_S \left(\frac{4L\rho t}{\left(L^2 + 4\rho^2\right)^{3/2}} \right)$$

Here, γ and J_S are defined as previously but now L represents the tube length, 2ρ is its diameter, and t is its wall thickness. Again for simplicity a thin-walled structure with $t << L \approx 2\rho$ has been assumed. Analogously to the double-disk structures, the field magnitude can be controlled by changing the tube length, the tube diameter, the tube wall thickness, or the magnetic material from which the tubes are made.

Interestingly, uniform field regions can also be created by asymmetric structures. An example of this is open elliptical shell structures that have their inner and outer boundaries defined by ellipsoids of differing eccentricities [127]. As surfaces of second degree, ellipsoids offer truly uniform internal magnetizations [128]. For

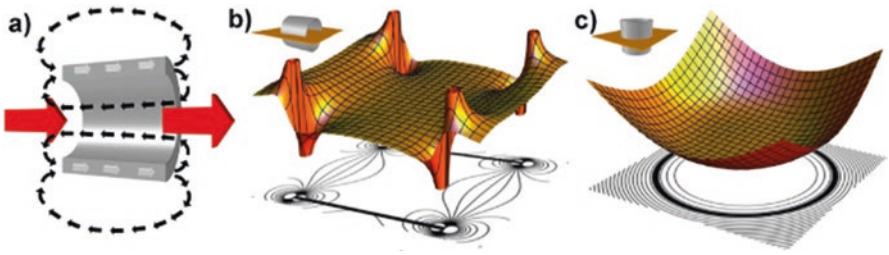

Fig. 2 Schematic of the fields generated by a magnetized hollow cylinder. (**a**) Cut-away schematic of the field (*black arrows*) of a hollow cylinder magnetized to saturation by that background MRI field (larger *red arrows*). (**b**) Calculated magnetic field magnitude profile with underlying field magnitude contour plot in a mid-plane through a magnetized hollow cylinder. Plane orientation shown in upper left corner. (**c**) As for (**b**) but for perpendicularly oriented mid-plane (reproduced in part from [126], with permission, IOP Publishing)

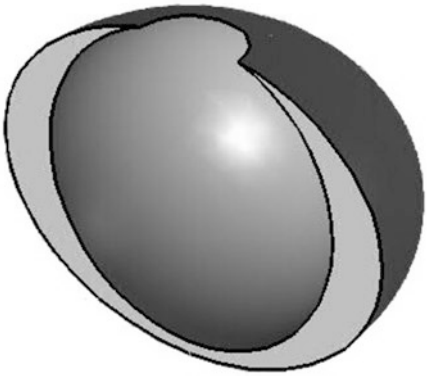

Fig. 3 Schematic of open, asymmetric ellipsoidal shell structure. Cross section through an open shell geometry defined by an oblate ellipsoid of revolution (oblate spheroid) after a vertically offset spherical volume has been removed

magnetically saturated ellipsoids, such uniform magnetization can be shown to result also for geometries that represent one ellipsoidal volume removed from within another, no matter whether the ellipsoidal volumes share a common center [127]. Thus various counterintuitive asymmetrical structures become possible, an example schematic being shown in Fig. 3. For these elliptical shell agents, the internal uniform field magnitudes and resulting frequency shifts depend on the difference in aspect ratios, or eccentricities, of the ellipsoidal shapes that define the structures' physical boundaries. A relatively simple case is a hollow shell structure formed by subtracting a spherical volume (of any radius r) from within an ellipsoid of revolution with semi-axes $r(1+\varepsilon_a)$ and $r(1+\varepsilon_b)$; frequency shifts are described by [127]

$$\Delta\omega \approx -\gamma J_S \left(\frac{4\left(\varepsilon_a - \varepsilon_b\right)}{15} \right)$$

where for simplicity again, a thin shell structure has been chosen with ε_a and ε_b much less than unity. Here, field magnitudes and NMR frequency shifts can be controlled by changing boundary ellipticities, by changing the size of either outer or inner bounding ellipsoid (thus changing shell "thickness"), or by changing the magnetic material from which the ellipsoidal shell is constructed.

As magnetic particles, all of these structures double as T_2 contrast agents. Indeed, one can imagine transforming a T_2 agent into a multispectral agent simply by redistributing its material, reforming the spherical (or randomly shaped) particle into a double-disk, hollow cylinder, elliptical shell, or any other shape capable of generating the necessary magnetic field profiles. No new magnetic material needs to be added or removed in the process. Since microparticle T_2 relaxation is dominated by transverse dephasing in the far field where particle shape is irrelevant, a multispectral microparticle agent created in this way would possess the same relaxing ability of the original microparticle agent. But by adding a local uniform field region, the material redistribution adds shape-identifying spectral information that enables particles that would otherwise appear identical in an MRI scan to be distinguished from one another.

Such particles therefore make interesting candidate labels for MRI-based cell tracking, a growing MRI application that may be of considerable value to new cell-based medical therapies [129, 130]. If surface functionalized such that different microstructure geometries target different cell types, labeled cells could be tracked using regular T_2*-weighted gradient echo imaging protocols, but also distinguished from one another through the geometrically encoded spectral content of their magnetic labels. Added spectral content could also distinguish hypointense image regions due to the administered contrast agent from those due to natural image darkenings or signal voids arising from air bubbles or other magnetic field inhomogeneities. Such "color" particle distinction can be seen in Fig. 4, which shows different resulting frequency shifts from double-disk structures with different disk thicknesses.

4.3 Frequency-Shifting Properties

Figure 5 displays several scanning electron micrograph (SEM) images of microfabricated magnetic double-disk, hollow cylinder, and ellipsoidal shell sample structures. Although geometrically distinct from one another, the shapes are unified through their frequency shifts that all reduce to

$$\Delta\omega \approx -\gamma J_S X$$

where X represents the bracketed portions in the equations above. As can be seen, in all cases X is a dimensionless function of solely the structure geometry. That is, at least as far as the magnetics are concerned (although not necessarily as far as the dynamics are concerned), shape-based frequency shifting is in principle scale invariant. Isotropically expanding or contracting any of the structures does not change the frequency shift, allowing agents to be produced over a large size range for different potential applications. Being independent of any chemical exchange processes and with material dependences appearing only through the gyromagnetic ratio and magnetic saturation polarization density, structures can also be used with any NMR-active medium and made from any magnetic material. This allows agents to be made from less toxic materials than the lanthanide ions used in PARACEST and clinical T_1 agents, which require powerful chelating ligands to protect the body from direct exposure [131]. To date, shaped particle agents have been made from nickel [101, 126, 127] as well as from more biocompatible materials including iron [132] and iron oxides [133]. They have also been shown to operate equally in water and in deuterium oxide [101], and have been produced with sizes ranging from milli- to micro- to nanoscale [101, 126, 134].

Lacking spherical symmetry, different particle orientations relative to the applied field can lead to different surrounding magnetic field profiles. These would change the resulting field shifts, were it not for the particles' self-aligning properties. Much

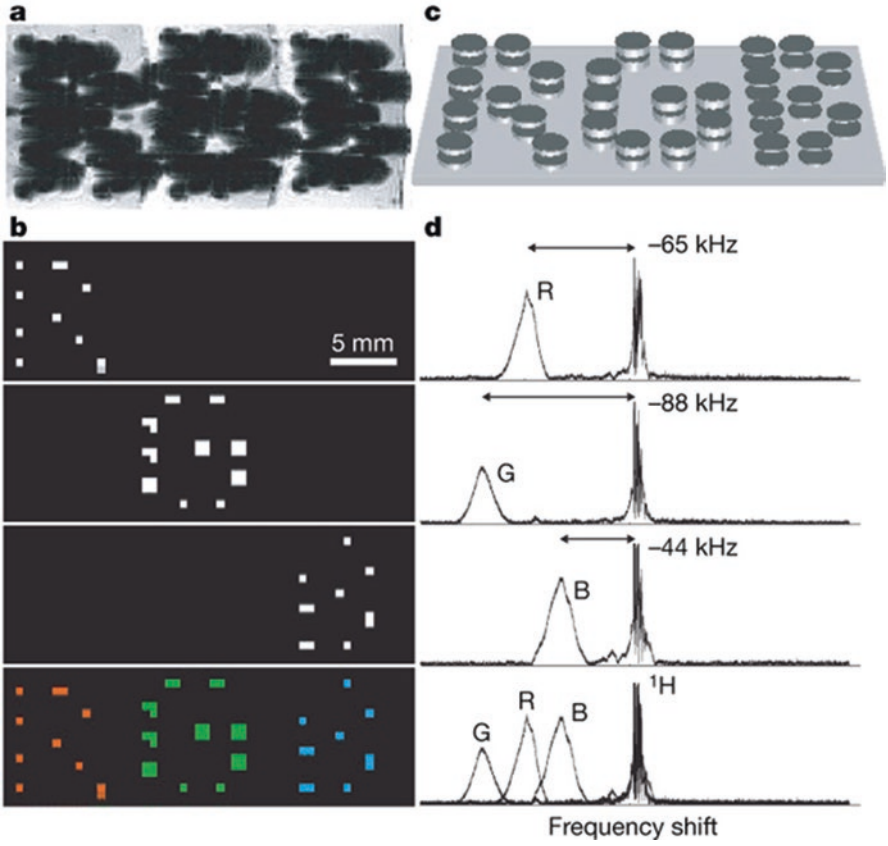

Fig. 4 Multispectral MRI. (**a**–**d**) Chemical shift imaging of demonstration 1.25 mm diameter particles magnetized by background MRI field. Particle frequency was varied by changing the thickness of electroplated nickel layers that formed the magnetizable disk pairs. As with normal magnetic particle detection, magnetic dephasing due to the particles' external fields enables the spatial imaging shown in the gradient-echo MRI (**a**). However, comparison between (**a**) and the chemical-shift images (**b**) shows that the additional spectral information both differentiates between particle types and improves particle localization. The particles are shown schematically (not to scale) in (**c**). With particle spectra (**d**), to the right of the corresponding chemical-shift images in (**b**) shifted well clear of the water proton line, different planes in the chemical-shift imaging map isolate different particle types for unambiguous color coding with minimal background interference (**b**, *bottom panel*). (Although still visible in the gradient-echo image, the top-corner particle of the letter "B" was damaged, causing its shifted frequency peak to vanish) (reproduced from [101], with permission, Nature Publishing Group)

like a compass needle in the earth's field, the particles' magnetic shape anisotropy causes strong magnetic torques that automatically align the particles parallel to one another when placed into the large fields of an MRI scanner [101]. This avoids random spread in resulting resonance shifts that might otherwise hinder the ability to distinguish different particle geometries.

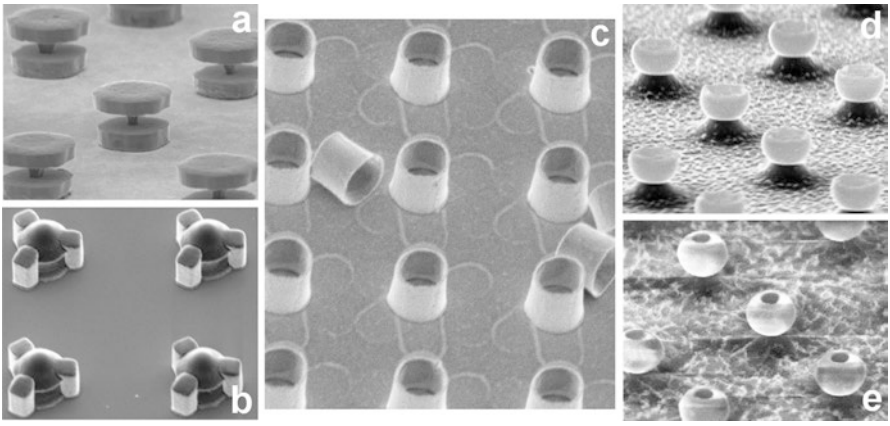

Fig. 5 Scanning electron micrographs (SEM) of microfabricated contrast agent microstructures. (**a**, **b**) SEM of magnetic double-disk structures separated by nonmagnetic internal or external spacing posts, respectively. (**c**) SEM of hollow magnetic cylinders. (**d**, **e**) SEM of open oblate and prolate ellipsoidal magnetic shells, respectively. For scale, all structures are a few micrometer in total size

Because particles can be made with ferromagnetic materials, which have far greater magnetic permeabilities than para- or diamagnetic materials, the range of accessible frequency shifts is large. Iron has a J_S value of over 2 T, for example, allowing NMR shifts for water protons to be engineered anywhere from zero up to tens of MHz. (In theory, shifting up to 100 MHz is possible, albeit only for unwieldly structures with very thick magnetic layers.) But even at 1 MHz or a fraction thereof, shifts easily exceed anything yet achieved with molecular agents.

Unlike paramagnetic (or diamagnetic) CEST agents, shifts generated by microparticle structures can also be field independent because typical MRI field strengths magnetically saturate the constituent ferromagnetic materials. Large field-independent shifts are advantageous because they raise the possibility of using such agents at clinical field strengths, rather than at the higher field strengths used to increase the shifts of molecular based (PARA)CEST agents. Whereas most chemical shifts are proportional to the MRI field and thus reported in relative terms of parts per million (ppm), for these shaped particle agents NMR shifts are absolute. In conventional, relative terms their shifts will therefore appear to change based on the applied field but, to aid comparison, for a 1.5 T clinical field strength MRI scanner, a MHz shift corresponds to around 15,000 ppm. Chemical shifts in NMR spectroscopy, by contrast, typically measure just a few ppm. Frequency shifting far from the background bulk water relaxes bandwidth constraints on the off-resonance radiation pulses used to address these agents. With little chance of any RF power leaking over to excite the background water, it enables virtually background-free imaging. That is, even though the signal still comes from water surrounding the magnetic particle rather than from the particle itself, the large shifts enable a form of "hotspot" imaging [135], different in mechanism, but not unlike that reported with highly shifted proton

(HSP) MR imaging [136] or with background-free imaging of ^{19}F labels. Based on magnetic nano- or microparticles that interact with surrounding water, these agents do however offer higher sensitivity than HSP or ^{19}F imaging, in large part due to their large frequency shifts that also enable significant signal amplification.

4.4 Diffusion-Driven Signal Amplification

In some cases, the frequency-shifted signals encoded by shaped magnetic nano- and microstructures can be directly imaged via chemical-shift imaging, a standard MRI protocol that spatially maps NMR frequencies. An instance of this was already shown in Fig. 4. Just like any other magnetic particles the shaped structures appear indistinguishable in a T_2-weighted gradient echo image. But in a chemical-shift image they are clearly distinguished from one another (as well as from the background water) through their ability to locally frequency-shift the nearby water by different amounts. Also clear, however, is that the frequency-shifted signals cover smaller areas than do the T_2 contrast signals. This is because the frequency shifting occurs within the particles' homogeneous field regions, which are small compared to the far-field volume over which water is transversely dephased. This means that shaped particles can be better spatially localized through their added spectral content, but it also means that their spectrally distinguishing signals are not as strong as their associated T_2 contrast signals.

To boost spectral signals, therefore, a variation of magnetization transfer imaging [137] is used, not unlike that employed for amplifying CEST-based signals. Here though, proton exchange does not imply chemical exchange. Instead exchange is driven by water self-diffusion that randomly moves water molecules into and out of the homogeneous field region. The particles' open structure design exploits this natural water diffusion to continually refresh protons contained with the field-shifted region. This yields an effective water volume from which signal can be acquired that may be several orders of magnitude larger than the homogeneous field region itself. That is, signal can be acquired not just from water that happens to be in the field-shifted region at one point in time, but from water passing through that region over an extended time period (of order the bulk-water longitudinal relaxation time, T_1).

The signal acquisition protocol is similar to that of CEST agents. A series of presaturating RF pulses, applied at a specific offset frequency from the background water resonance, are followed by a single on-resonance pulse and the resulting free induction decay (FID) signal used to infer the resulting reduction in the bulk water signal. This process can then be repeated for different offset frequencies, building up a z-spectrum that reveals the particle-induced shifted resonance through a spectrally localized dip in the remaining water signal. (Examples of such NMR z-spectra can be found later in Fig. 6.) Alternatively, knowing contrast particles' specific offset resonance frequencies allows for selectively addressable contrast that can be turned off and on.

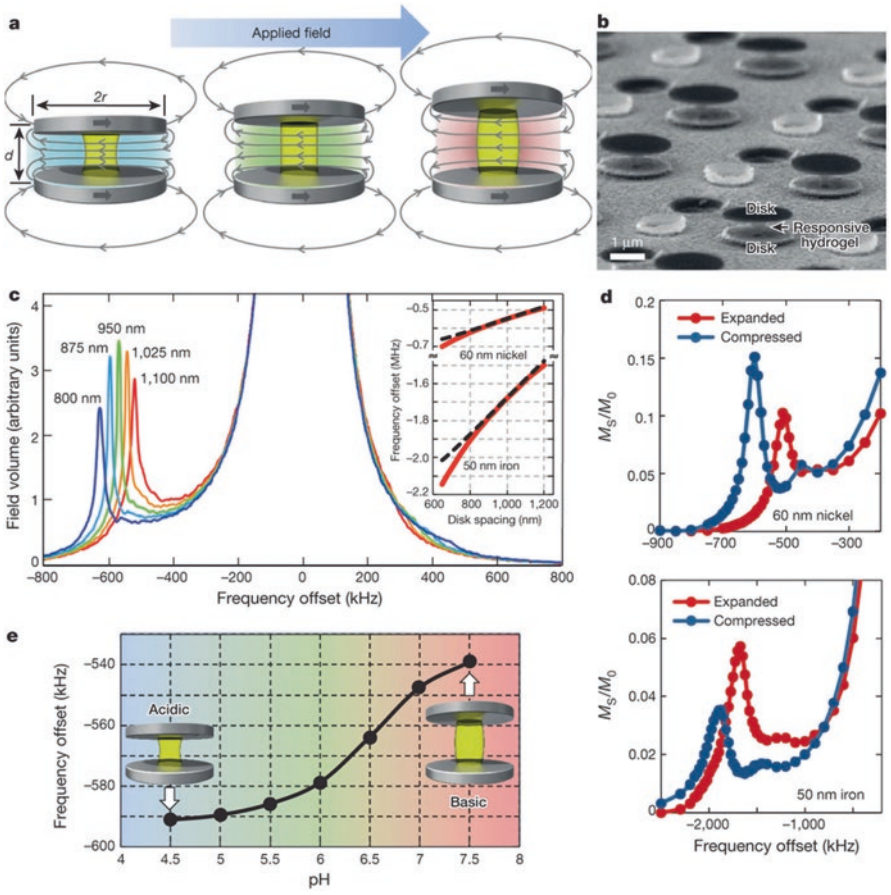

Fig. 6 Principles of shape-changing RF colorimetric sensors. (**a**) Schematic of sensor assemblies comprising two parallel disks magnetized by applied MRI field (*blue arrow*) and separated by stimuli-responsive hydrogel spacers (*yellow*). Resulting magnetic fields (*grey curves*) are uniform between the disks and locally shifted NMR frequencies of water passing through proportionally to the field magnitude, which depends on disk spacing *d*. Different frequency shifts represent different effective RF "colors." (**b**) Scanning electron micrograph of sensors. (Interspersed features are nonmagnetic residual topography from the microfabrication process.) (**c**) Theoretical precession frequency (or equivalently, field) histograms, mimicking NMR spectra, for 60 nm thick, 1 μm radius nickel disk pairs with disk spacing indicated. Background water appears at zero offset; shifted peaks result from uniform field regions between the disks. Inset: frequency offset versus disk spacing for nickel and iron disks with thicknesses shown. *Dashed black curves* are analytic approximations (see equation (1) in ref. [132]); *red curves* result from numerical field simulations. (**d**) Experimental NMR z-spectra for nickel (*top*) and iron (*bottom*) sensors with hydrogel spacers in compressed and expanded states. Magnetization saturated out M_S is normalized to the initial water magnetization M_0. (**e**) Experimental pH-dependent NMR shifts for nickel-based sensors containing pH-sensitive hydrogel spacers designed to shrink (expand) at low (high) pH with peak sensitivity in the physiological pH range (reproduced from [132], with permission, Nature Publishing Group)

Where shaped-particle signal amplification differs from that of molecular-based chemical exchange is in the number of, and the rate at which, protons that can be exchanged. Unlike chemical exchange processes, in which only a fraction of a molecule's protons are able to participate, with shaped particles most of the uniformly field-shifted volume of water can be exchanged simultaneously. Exchange rates are also no longer dependent on chemical rate constants; they depend on the time it takes water to self-diffuse through the particle's field-shifted region. Since diffusion distances scale with the square root of time, the exchange rate speeds up quadratically as particle sizes shrink, increasing the total signal that can be acquired. That is, while frequency shifts are independent of overall particle size, diffusion-driven signal amplification favors smaller (and less biologically invasive) particles.

Increasing exchange rates do increasingly broaden the shifted resonance linewidth. As mentioned with regard to CEST imaging, for agents to be effective, this broadening, which is proportional to the exchange rate, should not become so large that the shifted resonance overlaps with the unshifted background water [93]. Being ferromagnetic, particle agents offer larger frequency shifts than paramagnetic molecules, thus allowing higher exchange rates, which increase signal and should allow particles to be scaled down to below 100 nm in size. Taken together, shaped particles allow more protons to be simultaneously exchanged and allow those exchanges to recur more rapidly, yielding signal amplification and resulting contrast agent sensitivities that compare favorably with commonly used clinical T_1 agents [132].

5 Geometrically Based MRI Sensing

Just as optically based fluorescent tags and labels were soon followed by fluorescent sensors, MRI contrast agents have since expanded to include responsive MRI probes [138]. Such agents change surrounding image contrast in response to some chosen biomarker, which may include various biologically significant metal ions, biomolecules, or surrounding environmental conditions such as temperature or pH. Examples include changes in T_1 due to modified water access to the Gd ions [139], switches in T_2 due to induced aggregation of magnetic nanoparticles [78], changes in CEST contrast due to modified proton exchange rates [140], and signal switching in shaped particle structures by (un)blocking their homogeneous shifted field regions [101].

Whether based on T_1, T_2, CEST, or shaped particles, these sensing examples all amount to changes in the amplitude of the contrast agent signal. As mentioned, however, such signal changes cannot necessarily be distinguished from more mundane changes in the contrast agent concentration. For in vitro tests, concentrations may be well controlled, but this is not always true for in vivo studies where precise trafficking and pharmacokinetics of the administered contrast agents may be poorly known. An option is to administer two different contrast agents [141]. By assuming that at least the ratio of their concentrations remains constant, unwanted concentration dependences can be eliminated. But such ratiometric correction may require

larger overall amounts of exogenous agent and may still fail if there is any difference in agent pharmacokinetics.

One way to avoid ambiguity is through a responsive probe that reports via changes in NMR signal frequency rather than amplitude. Unlike signal amplitudes, NMR frequencies need not depend on contrast agent concentrations, allowing for more quantitative measurements. With resonant frequency shifts that can be directly engineered through particle geometry, multispectral shaped-particle contrast agents are well suited to the task. Converting such contrast agents into sensing agents is conceptually simple, requiring only a modified structure whose shape is no longer static, but can dynamically vary in an appropriate way in response to the chosen biomarker. As the structure changes shape, its surrounding magnetic field profile changes, in turn changing the local frequency shift imparted on the surrounding water signal. Given the large frequency shifts of shaped-particle agents, resulting responsive changes in those frequency shifts can be similarly large, in principle enabling even small biomarker changes to be detected.

The first such shape-changing, frequency-based, MRI sensor agents have only recently been published [132]. Referred to as Geometrically Encoded Magnetic (GEM) sensors, they employ stimulus-responsive polymer gels that effect the necessary shape changes and that enable continuous and reversible operation. (Interestingly, Paul Lauterbur, one of the original inventors of MRI, first proposed using a gel-based agent over two decades ago [142]. Except, without specific control over their magnetic fields, those agents yielded particle aggregation-dependent changes in relaxation, or signal amplitude, much like relaxation switch sensors [78].) The first examples of sensors that controllably change fields and therefore frequencies, however, used acid-sensitized hydrogels [143] to transduce local pH levels into NMR-readable frequency shifts. These sensors borrowed from the double-disk multispectral MRI agent geometry, using this time nanoscopic hydrogel pillars as spacing elements between the two magnetic disks. As these spacers swell or shrink in response to the pH of the surrounding solution, the attached disks move further apart or closer together. The resulting change in magnetic field magnitude between the disks then manifests as a changed offset resonance frequency for water passing between the disks, as detailed in Fig. 6. Since hydrogels can expand or contract by large amounts and since frequency changes can be shown to be proportional to length changes in the hydrogels separating the disks [132], large stimulus-induced spectral shifts are possible. Although stimuli-reponsive hydrogels, which rely on solute diffusion through the gel, offer notoriously slow macroscopic response times, for the nanoscopic hydrogel elements incorporated into the GEM sensors diffusion times are rapid, enabling sub-second response times.

As their name suggests, GEM sensors depend on geometry. Like the originating multispectral shaped-particle MRI contrast agents, GEM sensor signals are an intrinsic function of the shapes of the nanostructures involved. They afford not just another example of how particle shape enables new functionality, but of how the shape itself can function as a reporter of local conditions, which may extend beyond pH to include reporting on many other conditions and/or biomolecules of interest. Many different hydrogel formulations—many of them biocompatible—have

already been developed in other fields and there exists considerable literature demonstrating the ability to sensitize them to many variables of interest [144]. (Nor are hydrogels the only possible polymers that could be used to effect the necessary shape changes.) Gel sensitization techniques include molecular imprinting of gels [145], the incorporation of catalytic enzymes [146] or enzyme-cleavable substrates [147], and the inclusion of specific receptor-ligand-type recognition bondings [148]. By using hydrogels with responses tailored to different targets, the same geometrically based sensing platform should be adaptable to measure a variety of biomarkers. The multispectral nature of these agents suggests also that multiple different biomarkers might be measured simultaneously by using multiple different GEM sensors. Provided that these sensors are engineered with different initial frequency offsets, different sensor signals can be spectrally isolated from one another even if spatially co-located. This may allow for different sensors to be calibrated against each other and/or for panels of biomarkers to be measured simultaneously to better discriminate between pathologies.

6 Particle Synthesis

A distinguishing feature of shaped particle agents is their synthesis. MRI contrast agents have always been produced by bottom-up chemical synthesis routes; shaped agents have instead leveraged top-down microfabrication techniques [149]. They are produced using the same technology that underpins the electronics revolution and the ever-present, but ever-shrinking, integrated circuit. Supported by an indomitable semiconductor industry, investment in micro- and nanofabrication research over many years has resulted in powerful sets of tools, able to pattern materials with features that are now reaching less than a hundred atoms on a side. Although not used before for contrast agent synthesis, the extraordinary control that such tools offer over both structure shape and composition makes them a good choice for a contrast agent whose function depends on its geometry and material makeup. Of course, an MRI contrast agent is quite different from an integrated circuit and their microfabrication does require adaptation of traditional microfabrication protocols, but several routes have already been proven [126, 127, 132, 133, 150].

Top-down fabrication is not without its limitations, however. As the billions of transistors in each of today's billions of smartphones abundantly prove, top-down microfabrication is well suited to the creation of very small, very precise structures in a massively parallel manner. But throughput still cannot match that possible through bottom-up chemical synthesis, which may lack the precision, but which can produce large volumes of particles at a time. And even though resulting microfabricated components need not be expensive, the necessary microfabrication tools themselves are sometimes out of reach of academic labs, limiting the number of researchers that might otherwise be able to further develop particle-based multispectral contrast agent technology. Ironically then, while microfabrication is a key, enabling technology for proof-of-principle demonstrations of new structures and

new functionalities, a current handicap of such structures may be precisely their dependence on such technology.

An open question remains whether it might be possible to chemically synthesize all or some of the above shaped contrast agent structures with sufficient geometrical accuracy and size monodispersity. Having resonance frequencies determined by structure shapes allows differently "colored" agents to be engineered; but it also means that any errors in particle geometry, or variations in shape across a batch of particles, can reduce or blur their distinguishing spectral signals. Precise shape control can be difficult through bottom-up synthesis and monodispersity often deteriorates as particle sizes increase beyond a few tens of nanometer in size. But this is not to say that it is impossible either. Given the particles' large frequency-shifted signals, some trade-off between simplicity of particle synthesis and resulting spectral resolution may be acceptable. As the above particle zoo indicates, skill in the bottom-up chemical control of shapes is also quickly growing. Or perhaps hybrid template-based syntheses might offer simpler approaches. Although lower throughput than bottom-up chemical synthesis, they might nonetheless yield particles in reasonable quantity, particularly if compatible with some form of roll-to-roll processing [151].

7 Conclusion

In some ways, shaped agents can be regarded as a mix between particle-based T_2 and molecular-based (PARA)CEST agents, borrowing advantages from both. Based on magnetic particles, they provide T_2 contrast while remaining selectively addressable through frequency-shifted signals similar to those of CEST agents. In principle they can be made from exactly the same material as a T_2 agent, just reshaped to add identifying spectral content. And they can be imaged through similar gradient-echo T_2-weighted pulse sequences while their spectral information is acquired via similar signal-amplifying magnetization transfer protocols used with CEST agents, just driven now by diffusion, rather than chemical exchange.

But there are differences too. Deliberately shaped nano- and microparticles represent a considerable departure from traditional MRI contrast agents, an approach that may still be too new for its potential, or its pitfalls, to be fully appreciated yet. Their more controlled synthesis through top-down microfabrication has enabled new particle functionality and allowed precise tuning of desired contrast properties. But less accessible fabrication equipment has thus far also limited uptake in the community, retarding what might otherwise be more rapid development of the technology and fuller exploration of its potential. Currently, at around a micrometer in size, the shaped agents are also still relatively large compared to most (though not all) other MRI contrast agents. This need not necessarily be a detriment [152]. Their size may already be adequate for cell tracking studies—indeed, cell viability and tracking have already been tested using larger chemically synthesized spherical particles [63]. But to increase biological utility and reduce size-related biological deliv-

ery issues, sizes will ultimately need to be reduced further. This is not impossible: in theory, agents should continue to function down to below 100 nm size scales, but such agents must still be developed and proven in practice.

Exactly how and where such new shaped agents may find their largest impact is therefore still unclear. Possibly new classes of structures with new properties still await discovery. Viewing them as RF analogs to quantum dot or plasmonic nanoparticles suggests a variety of potential applications within biology and beyond. What does seem already clear, however, is that magnetic particle shape, not just size, enables novel imaging and sensing functionalities, offering new avenues to explore in the burgeoning field of nanoparticle-based biomedical imaging.

References

1. Tsien RY. The green fluorescent protein. Ann Rev Biochem. 1998;67:509–44.
2. Giepmans BNG, Adams SR, Ellisman MH, Tsien RY. Review—the fluorescent toolbox for assessing protein location and function. Science. 2006;312:217–24.
3. Chalfie M, Tu Y, Euskirchen G, Ward WW, Prasher DC. Green fluorescent protein as a marker for gene-expression. Science. 1994;263:802–5.
4. Betzig E, et al. Imaging intracellular fluorescent proteins at nanometer resolution. Science. 2006;313:1642–5.
5. Huang B, Bates M, Zhuang X. Super-resolution fluorescence microscopy. Ann Rev Biochem. 2009;78:993–1016.
6. Bruchez Jr M, Moronne M, Gin P, Weiss S, Alivisatos AP. Semiconductor nanocrystals as fluorescent biological labels. Science. 1998;281:2013–6.
7. Alivisatos P. The use of nanocrystals in biological detection. Nat Biotechnol. 2004;22:47–52.
8. Chan WCW, Nie S. Quantum dot bioconjugates for ultrasensitive nonisotopic detection. Science. 1998;281:2016–8.
9. Michalet X, et al. Quantum dots for live cells, in vivo imaging, and diagnostics. Science. 2005;307:538.
10. Anker JN, et al. Biosensing with plasmonic nanosensors. Nat Mater. 2008;7:442.
11. Hu M, et al. Gold nanostructures: engineering their plasmonic properties for biomedical applications. Chem Soc Rev. 2006;35:1084–94.
12. Fu CC, et al. Characterization and application of single fluorescent nanodiamonds as cellular biomarkers. Proc Natl Acad Sci U S A. 2007;104:727–32.
13. Lim SY, Shen W, Gao Z. Carbon quantum dots and their application. Chem Soc Rev. 2015;44:362–81.
14. Pederson JA, Swartz MA. Mechanobiology in the third dimension. Ann Biomed Eng. 2005;33:1469–90.
15. Ntziachristos V. Going deeper than microscopy: the optical imaging frontier in biology. Nat Methods. 2010;7:603–14.
16. Webb RH. Confocal optical microscopy. Rep Prog Phys. 1996;59:427–71.
17. Helmchen F, Denk W. Deep-tissue two-photon microscopy. Nat Methods. 2005;2:932–40.
18. Zipfel WR, Williams RM, Webb WW. Nonlinear magic: multiphoton microscopy in the biosciences. Nat Biotechnol. 2003;21:1368–76.
19. Ntziachristos V, Ripoll J, Wang LHV, Weissleder R. Looking and listening to light: the evolution of whole-body photonic imaging. Nat Biotechnol. 2005;23:313–20.
20. Mosk AP, Lagendijk A, Lerosey G, Fink M. Controlling waves in space and time for imaging and focusing in complex media. Nat Photonics. 2012;6:283–92.

21. Katz O, Small E, Guan Y, Silberberg Y. Noninvasive nonlinear imaging through strongly-scattering turbid layers. Optica. 2014;3:170–4.
22. Hilderbrand SA, Weissleder R. Near-infrared fluorescence: application to in vivo molecular imaging. Curr Opin Chem Bio. 2010;14:71.
23. Guo ZQ, Park S, Yoon J, Shin I. Recent progress in the development of near-infrared fluorescent probes for bioimaging. Chem Soc Rev. 2014;43:16–29.
24. Callaghan PT. Principles of nuclear magnetic resonance microscopy. New York: Oxford Univ. Press; 1991.
25. Moseley ME, et al. Diffusion-weighted MR imaging of anisotropic water diffusion in cat central-nervous-system. Radiology. 1990;176:439–45.
26. Basser PJ. Inferring microstructural features and the physiological state of tissues from diffusion-weighted images. NMR Biomed. 1995;8:333–44.
27. LeBihan D, et al. Diffusion tensor imaging: concepts and applications. J Magn Reson Imag. 2001;13:534–46.
28. Haacke EM, Xu YB, Cheng YCN, Reichenbach JR. Susceptibility weighted imaging (SWI). Magn Reson Med. 2004;52:612–8.
29. Calamante F, Thomas DL, Pell GS, Wiersma J, Turner R. Measuring cerebral blood flow using magnetic resonance imaging techniques. J Cereb Blood Flow Metab. 1999;19:701–35.
30. Detre JA, Leigh JS, Williams DS, Koretsky AP. Perfusion imaging. Magn Reson Med. 1992;23:37–45.
31. Ogawa S, Lee TM, Nayak AS, Glynn P. Oxygenation-sensitive contrast in magnetic-resonance image of rodent brain at high magnetic fields. Magn Reson Med. 1990;14:68–78.
32. Sosnovik DE, Weissleder R. Emerging concepts in molecular MRI. Curr Opin Biotechnol. 2006;18:4–10.
33. Sipkins DA, Cheresh DA, Kazemi MR, Nevin LM, Bednarski MD, Li KC. Detection of tumor angiogenesis in vivo by $alpha_V beta_3$-targeted magnetic resonance imaging. Nat Med. 1998;4:623–6.
34. Yu X, et al. High-resolution MRI characterization of human thrombus using a novel fibrin-targeted paramagnetic nanoparticle contrast agent. Magn Reson Med. 2000;44:867–72.
35. Flacke S, et al. Novel MRI contrast agent for molecular imaging of fibrin: implications for detecting vulnerable plaques. Circulation. 2001;104:1280–5.
36. Weissleder R, Reimer R, Lee AS, Wittenberg J, Brady TJ. MR receptor imaging—ultrasmall iron-oxide particles targeted to asialoglycoprotein receptors. Am J Roentgenology. 1990;155:1161–7.
37. Louie AY, et al. In vivo visualization of gene expression using magnetic resonance imaging. Nat Biotechnol. 2000;18:321–5.
38. Weissleder R, et al. In vivo magnetic resonance imagine of transgene expression. Nat Med. 2000;6:351–4.
39. Genove G, DeMarco U, Xu H, Goins WF, Ahrens ET. A new transgene reporter for in vivo magnetic resonance imaging. Nat Med. 2005;11:450–4.
40. Gilad AA, et al. Artificial reporter gene providing MRI contrast based on proton exchange. Nat Biotechnol. 2007;25:217–9.
41. Gilad AA, Ziv K, McMahon MT, van Zijl PCM, Neeman M, Bulte JWM. MRI reporter genes. J Nucl Med. 2008;49:1905–8.
42. Glunde K, Artemov D, Penet M-F, Jacobs MA, Bhujwalla ZM. Magnetic resonance spectroscopy in metabolic and molecular imaging and diagnosis of cancer. Chem Rev. 2010;110:3043.
43. Mountford CE, Stanwell P, Lin A, Ramadan S, Ross B. Neurospectroscopy: the past, present and future. Chem Rev. 2010;110:3060–86.
44. Nelson KL, Runge VM. Basic principles of MR contrast. Topics Magn Reson Imaging. 1995;7:124–36.
45. Merbach A, Helm H, Tóth E, editors. The chemistry of contrast agents in medical magnetic resonance imaging. 2nd ed. West Sussex, UK: Wiley; 2013.
46. Watanabe M, Tanaka R, Takeda N. Magnetic-resonance-imaging and histopathology of cerebral gliomas. Neuroradiology. 1992;34:463–9.

47. Caravan P, Ellison JJ, McMurry TJ, Lauffer RB. Gadolinium(III) chelates as MRI contrast agents: structure, dynamics, and applications. Chem Rev. 1999;99:2293–352.
48. Bottrill M, Kwok L, Long NJ. Lanthanides in magnetic resonance imaging. Chem Soc Rev. 2006;35:557–71.
49. Rocklage SM, Cacheris WP, Quay SC, Hahn FE, Raymond KN. Manganese(II) n, n′-dipyrid oxylethylenediamine-n, n′-diacetate 5,5′-bis(phosphate)—synthesis and characterization of a paramagnetic chelate for magnetic-resonance imaging enhancement. Inorg Chem. 1989;28: 477–85.
50. Koretsky AP, Silva AC. Manganese-enhance magnetic resonance imaging. NMR Biomed. 2004;17:527–31.
51. Silva AC, Lee JH, Aoki I, Koretsky AP. Manganese-enhanced magnetic resonance imaging (MEMRI): methodological and practical considerations. NMR Biomed. 2004;17:532–43.
52. Na HB, et al. Development of a T-1 contrast agent for magnetic resonance imaging using MnO nanoparticles. Angew Chem Int Ed. 2007;46:5397–401.
53. Gilad AA, et al. MR tracking of transplanted cells with "positive contrast" using manganese oxide nanoparticles. Magn Reson Med. 2008;60:1–7.
54. Park JY, et al. Paramagnetic ultrasmall gadolinium oxide nanoparticles as advanced T-1 MR1 contrast agent: account for large longitudinal relaxivity, optimal particle diameter, and in vivo T-1 MR images. ACS Nano. 2009;3:3663–9.
55. Engstrom M, Klasson A, Pedersen H, Vahlberg C, Kall PO, Uvdal K. High proton relaxivity for gadolinium oxide nanoparticles. Magn Reson Mat Phys Bio Med. 2006;19:180–6.
56. Hyeon T. Chemical synthesis of magnetic nanoparticles. Chem Commun. 2003;8:927–34.
57. Gupta AK, Gupta M. Synthesis and surface engineering of iron oxide nanoparticles for biomedical applications. Biomaterials. 2005;26:3995–4021.
58. Shen T, Weissleder R, Papisov M, Bogdanov Jr A, Brady TJ. Monocrystalline iron oxide nanocompounds (MION): physicochemical properties. Magn Reson Med. 1993;29:599–604.
59. Weissleder R, Elizondo G, Wittenberg J, Rabito CA, Bengele HH, Josephson L. Ultrasmall superparamagnetic iron oxide: characterization of a new class of contrast agents for MR imaging. Radiology. 1990;175:489–93.
60. Bulte JWM, et al. Magnetodendrimers allow endosomal magnetic labeling and in vivo tracking of stem cells. Nat Biotech. 2001;19:1141–7.
61. Jung CW, Jacobs P. Physical and chemical properties of superparamagnetic iron oxide MR contrast agents: ferumoxides, ferumoxtran, ferumoxsil. Magn Reson Imaging. 1995;13: 661–74.
62. Wang YX, Hussain SM, Krestin GP. Superparamagnetic iron oxide contrast agents: physicochemical characteristics and applications in MR imaging. Eur Radiol. 2001;11:2319–31.
63. Shapiro EM, Skrtic S, Koretsky AP. Sizing it up: cellular MRI using micron-sized iron oxide particles. Magn Reson Med. 2005;53:329–38.
64. Shapiro EM, Skrtic S, Sharer K, Hill JM, Dunbar CE, Koretsky AP. MRI detection of single particles for cellular imaging. Proc Natl Acad Sci. 2004;101:10901–6.
65. Seppenwoolde J-H, Viergever MA, Bakker CJG. Passive tracking exploiting local signal conservation: the white marker phenomenon. Magn Reson Med. 2003;50:784–90.
66. Cunningham CH, Arai T, Yang PC, McConnell MV, Pauly JM, Conolly SM. Positive contrast magnetic resonance imaging of cells labeled with magnetic nanoparticles. Magn Reson Med. 2005;53:999–1005.
67. Bellin MF, Zaim S, Auberton E, Sarfati G, Duron JJ, Khayat D, Grellet J. Liver metastase—safety and efficacy of detection with superparamagnetic iron-oxide in MR-imaging. Radiology. 1994;193:657–63.
68. Weinmann HJ, Ebert W, Misselwitz B, Schmitt-Willich H. Tissue-specific MR contrast agents. Eur J Radiol. 2003;46:33–44.
69. Frank JA, et al. Clinically applicable labeling of mammalian and stem cells by combining superparamagnetic iron oxides and transfection agents. Radiology. 2003;228:480–7.

70. Bulte JWM, Kraitchman DL. Iron oxide MR contrast agents for molecular and cellular imaging. NMR Biomed. 2004;17:484–99.
71. Modo M, Hoehn M, Bulte JWM. Cellular MR imaging. Mol Imaging. 2005;4:143–64.
72. Wu YL, Ye Q, Foley LM, Hitchens TK, Sato K, Williams JB, Ho C. In situ labeling of immune cells with iron oxide particles: an approach to detect organ rejection by cellular MRI. Proc Natl Acad Sci. 2006;103:1852–7.
73. Shapiro EM, Gonzalez-Perez O, Garcia-Verdugo JM, Alvarez-Buylla A, Koretsky AP. Magnetic resonance imaging of the migration of neuronal precursors generated in the adult rodent brain. Neuroimage. 2006;32:1150–7.
74. Dodd SJ, Williams M, Suhan JP, Williams DS, Koretsky AP, Ho C. Detection of single mammalian cells by high-resolution magnetic resonance imaging. Biophys J. 1999;76:103–9.
75. Hinds KA, et al. Highly efficient endosomal labeling of progenitor stem cells with large magnetic particles allows magnetic resonance imaging of single cells. Blood. 2003;102: 867–72.
76. Foster-Gareau P, Heyn C, Alejski A, Rutt BK. Imaging single mammalian cells with a 1.5 T clinical MRI scanner. Magn Reson Med. 2003;49:968–71.
77. Shapiro EM, Sharer K, Skrtic S, Koretsky AP. In vivo detection of single cells by MRI. Magn Reson Med. 2006;55:242–9.
78. Perez JM, Josephson L, O'Loughlin T, Högemann D, Weissleder R. Magnetic relaxation switches capable of sensing molecular interactions. Nat Biotechnol. 2002;20:816–20.
79. Sun EY, Weissleder R, Josephson L. Continuous analyte sensing with magnetic nanoswitches. Small. 2006;2:1144–7.
80. Tanimoto A, Pouliquen D, Kreft BP, Stark DD. Effects of spatial distribution on proton relaxation enhancement by particulate iron oxide. J Magn Reson Imaging. 1994;4:653–7.
81. Gilad AA, et al. MR tracking of transplanted cells with "positive contrast" using manganese oxide nanoparticles. Magn Reson Med. 2008;60:1–7.
82. Ruiz-Cabello J, Barnett BP, Bottomley PA, Bulte JWM. Fluorine (F-19) MRS and MRI in biomedicine. NMR Biomed. 2011;24:114–29.
83. Chen JJ, Lanza GM, Wickline SA. Quantitative magnetic resonance fluorine imaging: today and tomorrow. Wiley Interdiscip Rev Nanomed Nanobiotechnol. 2010;2:431–40.
84. Holland GN, Bottomley PA, Hinshaw WS. F-19 magnetic-resonance imaging. J Magn Reson. 1977;28:133–6.
85. Gallagher FA, et al. Magnetic resonance imaging of pH in vivo using hyperpolarized (13) C-labelled bicarbonate. Nature. 2008;453:940–3.
86. Golman K, Petersson JS. Metabolic imaging and other applications of hyperpolarized C-13. Acad Radiol. 2006;13:932–42.
87. Cassidy MC, Chan HR, Ross BD, Bhattacharya PK, Marcus CM. In vivo magnetic resonance imaging of hyperpolarized silicon particles. Nat Nanotech. 2013;8:363–8.
88. Partlow KC, et al. F-19 magnetic resonance imaging for stem/progenitor cell tracking with multiple unique perfluorocarbon nanobeacons. FASEB J. 2007;21:1647–54.
89. Ward KM, Aletras AH, Balaban RS. A new class of contrast agents for MRI based on proton chemical exchange dependent saturation transfer (CEST). J Magn Reson. 2000;143:79–87.
90. Zhang S, Merritt M, Woessner DE, Lenkinski RE, Sherry AD. PARACEST agents: modulating MRI contrast via water proton exchange. Acc Chem Res. 2003;36:783–90.
91. Grad J, Bryant RG. Nuclear magnetic cross-relaxation spectroscopy. J Magn Reson. 1990;90:1.
92. Zhou JY, Payen JF, Wilson DA, Traystman RJ, van Zijl PCM. Using the amide proton signals of intracellular proteins and peptides to detect pH effects in MRI. Nat Medicine. 2003;9:1085–90.
93. Woods M, Woessner DE, Sherry AD. Paramagnetic lanthanide complexes as PARACEST agents for medical imaging. Chem Soc Rev. 2006;35:500–11.
94. Aime S, Carrera C, Delli Castelli D, Crich SG, Terreno E. Tunable imaging of cells labeled with MRI-PARACEST agents. Angew Chem Int Ed. 2005;44:1813–5.

95. McMahon MT, Gilad AA, DeLiso MA, Cromer Berman SM, Bulte JWM, van Zijl PCM. New "multicolor" polypeptide diamagnetic chemical exchange saturation transfer (DIACEST) contrast agents for MRI. Magn Reson Med. 2008;60:803–12.
96. Nicholls FJ, Ling W, Ferrauto G, Aime S, Modo M. Simultaneous MR imaging for tissue engineering in a rat model of stroke. Sci Rep. 2015. doi: 10.1038/srep14597.
97. Aime S, Delli Castelli D, Terreno E. Supramolecular adducts between poly-L-arginine and [Tm^{III}dotp]: a route to sensitivity-enhanced magnetic resonance imaging-chemical exchange saturation transfer agents. Angew Chem Int Ed. 2003;42:4527.
98. Wu Y, et al. Polymeric PARACEST agents for enhancing MRI contrast sensitivity. J Am Chem Soc. 2008;130:13854.
99. Aime S, Delli Castelli D, Terreno E. Highly sensitive MRI chemical exchange saturation transfer agents using liposomes. Angew Chem Int Ed. 2005;44:5513–5.
100. Schröder L, Lowery TJ, Hilty C, Wemmer DE, Pines A. Molecular imaging using a targeted magnetic resonance hyperpolarized biosensor. Science. 2006;314:446–9.
101. Zabow G, Dodd S, Moreland J, Koretsky A. Micro-engineered local field control for high-sensitivity multispectral MRI. Nature. 2008;453:1058–63.
102. Sau TK, Rogach AL, editors. Complex-shaped metal nanoparticles: bottom-up syntheses and applications. Weinheim: Wiley; 2012.
103. Champion JA, Katare YK, Mitragotri S. Making polymeric micro- and nanoparticles of complex shapes. Proc Natl Acad Sci. 2007;104:11901–4.
104. Zhang XA, Elek J, Chang C-H. Three-dimensional nanolithography using light scattering from colloidal particles. ACS Nano. 2013;7:6212–8.
105. Narayanan R, El-Sayed MA. Shape-dependent catalytic activity of platinum nanoparticles in colloidal solution. Nano Lett. 2004;4:1343–8.
106. Grzelczak M, Vermant J, Furst EM, Liz-Marzan LM. Directed self-assembly of nanoparticles. ACS Nano. 2010;4:3591.
107. Ding T, Song K, Clays K, Tung C. Fabrication of 3D photonic crystals of ellipsoids: convective self-assembly in magnetic field. Adv Mater. 2009;21:1936.
108. Mittal M, Furst EM. Electric field-directed convective assembly of ellipsoidal colloidal particles to create optically and mechanically anisotropic thin films. Adv Funct Mater. 2009;19:3271.
109. Gratton SEA, et al. The effect of particle design on cellular internalization pathways. Proc Natl Acad Sci U S A. 2008;105:11613–8.
110. Champion JA. Mitragotri. Role of target geometry in phagocytosis. Proc Natl Acad Sci U S A. 2006;103:4930–4.
111. Chithrani BD, Ghazini AA, Chan WCW. Determining the size and shape dependence of gold nanoparticle uptake into mammalian cells. Nano Lett. 2006;6:662–8.
112. Park JH, et al. Systematic surface engineering of magnetic nanoworms for in vivo tumor targeting. Small. 2009;5:694–700.
113. Kolhar P, et al. Using shape effects to target antibody-coated nanoparticles to lung and brain endothelium. Proc Natl Acad Sci U S A. 2013;110:10753–8.
114. Kelly KL, et al. The optical properties of metal nanoparticles: the influence of size, shape, and dielectric environment. J Phys Chem B. 2003;107:668–77.
115. Wang YC, et al. Comparison study of gold nanohexapods, nanorods, and nanocages for photothermal cancer treatment. ACS Nano. 2013;7:2068–77.
116. Cole JR, Mirin NA, Knight MW, Goodrich GP, Halas NJ. Photothermal efficiencies of nanoshells and nanorods for clinical therapeutic applications. J Phys Chem C. 2009;113:12090–4.
117. Tottori S, et al. Magneti helical micromachines: fabrication, controlled swimming, and cargo transport. Adv Mater. 2012;24:811–6.
118. Kim DH, et al. Biofunctionalized magnetic-vortex microdiscs for targeted cancer-cell destruction. Nat Mater. 2010;9:165–71.
119. Martinez-Boubeta C, et al. Learning from nature to improve the heat generation of iron-oxide nanoparticles for magnetic hyperthermia applications. Sci Rep. 2013. Doi 10.1038/srep01652.

120. Shapiro EM, Koretsky AP. Convertible manganese contrast for molecular and cellular MRI. Magn Reson Med. 2008;60:265–9.
121. Zhao ZH, et al. Octapod iron oxide nanoparticles as high-performance T-2 contrast agents for magnetic resonance imaging. Nat Comm. 2013. doi 10.1038/ncomms3266.
122. Rotz MW, et al. High relaxivity Gd(III)-DNA gold nanostars: investigation of shape effects on proton relaxation. ACS Nano. 2015;9:3385–96.
123. Sitharaman B, et al. Superparamagnetic gadonanotubes are high-performance MRI contrast agents. Chem Comm. 2005;31:3915–7.
124. Sethi R, Mackeyev Y, Wilson LJ. The gadonanotubes revisited: a new frontier in MRI contrast agent design. Inorg Chim Acta. 2012;393:165–72.
125. Zabow G, Dodd SJ, Shapiro E, Moreland J, Koretsky AP. Microfabricated high-moment micrometer-sized MRI contrast agents. Magn Reson Med. 2011;65:645–55.
126. Zabow G, Dodd SJ, Moreland J, Koretsky AP. The fabrication of uniform cylindrical nanoshells and their use as spectrally tunable MRI contrast agents. Nanotechnology. 2009;20:385301.
127. Zabow G, Dodd SJ, Koretsky AP. Ellipsoidal microcavities: electromagnetic properties, fabrication, and use as multispectral MRI agents. Small. 2014;10:1902–7.
128. Maxwell JC. A treatise on electricity and magnetism, vol. 2. 3rd ed. Oxford: Clarendon; 1904.
129. Long CM, Bulte JWM. In vivo tracking of cellular therapeutics using magnetic resonance imaging. Expert Opin Biol Ther. 2009;9:293–306.
130. Ahrens ET, Bulte JWM. Tracking immune cells in vivo using magnetic resonance imaging. Nat Rev Immunol. 2013;13:755–63.
131. Hao DP, Ai T, Goerner F, Hu XM, Runge VM, Tweedle M. MRI contrast agents: basic chemistry and safety. J Magn Reson Imag. 2012;36:1060–71.
132. Zabow G, Dodd SJ, Koretsky AP. Shape-changing magnetic assemblies as high-sensitivity NMR-readable nanoprobes. Nature. 2015;520:73–7.
133. Wang X, Wang C, Anderson S, Zhang X. Microfabricated iron oxide particles for tunable, multispectral magnetic resonance imaging. Mater Lett. 2013;110:122–6.
134. Wang C, Wang X, Anderson S, Zhang X. Biocompatible, micro- and nanofabricated magnetic cylinders for potential use as contrast agents for magnetic resonance imaging. Sens Actuators B Chem. 2014;196:670–5.
135. Bulte JWM. Hot spot MRI emerges from the background. Nat Biotechnol. 2005;23:945–6.
136. Schmidt R, et al. Highly shifted proton MR imaging: cell tracking by using direct detection of paramagnetic compounds. Radiology. 2014;272:785–95.
137. Henkelman RM, Stanisz GJ, Graham SJ. Magnetization transfer in MRI: a review. NMR Biomed. 2001;14:57.
138. Yoo B, Pagel MD. An overview of responsive MRI contrast agents for molecular imaging. Front Biosci. 2008;13:1733–52.
139. Moats RA, Fraser SE, Meade TJ. A “smart” magnetic resonance imaging agent that reports on specific enzymatic activity. Angew Chem Int Ed. 1997;36:726–8.
140. Ward KM, Balaban RS. Determination of pH using water protons and chemical exchange dependent saturation transfer (CEST). Magn Reson Med. 2000;44:799–802.
141. Martinez GV, et al. Imaging the extracellular pH of tumors by MRI after injection of a single cocktail of T1 and T2 contrast agents. NMR Biomed. 2011;24:1380–91.
142. Frank S, Lauterbur PC. Voltage-sensitive magnetic gels as magnetic resonance monitoring agents. Nature. 1993;363:334–6.
143. Peppas NA, Hilt JZ, Khademhosseini A, Langer R. Hyrogels in biology and medicine: from molecular principles to bionanotechnology. Adv Mater. 2006;18:1345–60.
144. Ulijn RV, et al. Bioresponsive hydrogels. Mater Today. 2007;10:40.
145. Byrne ME, Park K, Peppas NA. Molecular imprinting within hydrogels. Adv Drug Deliv Rev. 2002;54:149–61.
146. Fischel-Ghodsian F, Brown L, Mathiowitz E, Brandenburg D, Langer R. Enzymatically controlled drug delivery. Proc Natl Acad Sci U S A. 1988;85:2403–6.

147. Plunkett KN, Berkowski KL, Moore JS. Chymotrypsin responsive hydrogel: application of a disulfide exchange protocol for the preparation of methacrylamide containing peptides. Biomacromolecules. 2005;6:632–7.
148. Miyata T, Asami N, Uragami T. A reversibly antigen-responsive hydrogel. Nature. 1999;399:766–9.
149. Madou MJ. Fundamentals of microfabrication and nanotechnology. 3rd ed. Boca Raton, FL: CRC Press; 2011.
150. Zabow G, Koretsky AP, Moreland J. Design and fabrication of a micromachined multispectral magnetic resonance imaging agent. J Micromech Microeng. 2009;19:025020.
151. Perry JL, Herlihy KP, Napier ME, Desimone JM. PRINT: a novel platform toward shape and size specific nanoparticle theranostics. Acc Chem Res. 2011;44:990–8.
152. Whitesides GM. The “right” size in nanobiotechnology. Nat Biotech. 2003;21:1161.